Phase-field modeling of anomalous spiral step growth on Si(001) surface

Yan-Mei Yu,[1,2,3] Bang-Gui Liu,[2,3] and Axel Voigt[1]

[1]*Institut für Wissenschaftliches Rechnen, Technische Universität Dresden, 01062 Dresden, Germany*
[2]*Institute of Physics, Chinese Academy of Science, P.O. Box 603, 100190 Beijing, China*
[3]*Beijing National Laboratory for Condensed Matter Physics, Beijing 100190, China*

Motivated by recent experimental results on anomalous spiral step motion on Si(001) surfaces, we use a phase-field model to understand the observed growth mode. The developed phase-field model allows simulation of step motion and surface phase switching for growth and sublimation. Our simulated results reproduce the anomalous spiral step motion on the Si(001) surfaces. Furthermore, we investigate the step dynamics in terms of the steady-state spiral shape for possible strain distributions and a large range of deposition rates. The obtained scaling law of the step spacing as a function of the deposition rate is different from earlier results for conventional spiral step growth, and indicates a crossover toward the local step dynamics due to the strain field of the screw dislocation on the Si(001) surfaces.

I. INTRODUCTION

Spiral step growth is a typical growth mode on atomically flat surfaces with screw dislocations. A step emerges from the exposed screw dislocation which cannot be removed by growth or evaporation. Under deposition the step turns around the exposed screw dislocation and forms a characteristic Archimedes spiral. Burton *et al.*[1] developed the earliest theory of spiral growth at the limit in which the step motion is controlled by local supersaturation of adatoms near the spiral ridge. In this limit the spiral step growth evolves into an Archimedes spiral with a steady-state spacing between two successive steps.[2] A scaling law of the steady-state step spacing l versus the deposition rate F can be found, describing the spiral step growth dynamics. In the presence of an Ehrlich-Schwoebel barrier, the spiral step growth deviates from the uniform step spacing and forms a typical mound shape with steep edges.[3] Both regimes can be found in practical applications; the models however neglect the influence of the strain field resulting from the screw dislocation. Taking these effects into account might lead to anomalous spiral step motion as recently found on a Si(001) surface.[4,5] The anomalous behavior was attributed to interaction between the surface structure and the strain field of the screw dislocation on the Si(001) surface. The screw dislocation breaks two single atomic-height steps. At each step, the surface phase switches between (1×2) and (2×1). The strain field of the screw dislocation causes an asymmetry of the two phases,[6,7] i.e., one phase is more energetically favored than the other. The step growth is coupled with the asymmetric phase switching between (1×2) and (2×1), causing the anomalous spiral profile. Even if a basic interpretation of the anomalous spiral step motion is available, the related dynamics still needs to be investigated further, especially at large time and space scales.

In this paper, we investigate the anomalous step motion on the Si(001) surface by using a phase-field model. Phase-field approach has already been applied to conventional spiral growth, surface phase transition, and island growth, where complex factors such as anisotropy, attachment kinetics, Ehrlich-Schwoebel barrier, and nucleation kinetics are incorporated successfully.[2,3,8–13] Here, we extend the phase-field description of the step motion by considering the surface phase switching between (1×2) and (2×1) during the surface growth and sublimation. Our simulations reproduce the anomalous spiral motion on the Si(001) surface. The steady-state spiral profile is investigated for possible strain distributions and a large range of deposition rates. A scaling law $l \sim F^{-0.41}$ is obtained for the anomalous spiral growth, which deviates from the prediction $l \sim F^{-1/3}$ for the general Archimedes spiral growth.[2] This indicates a crossover toward local step dynamics due to the strain field of the screw dislocation on the Si(001) surface.

The remaining part of this paper is organized as follows. In Sec. II we shall present our phase-field model and computational details. In Sec. III we shall present our simulated results and a discussion. In Sec. IV we shall give our main conclusion.

II. PHASE-FIELD MODEL

In the phase-field model we use a variable Φ to describe the surface height. Sharp transition zones of Φ describe steps between different terraces. The phase-field model is set on a square x-y domain, where x and y are the horizontal and vertical axes. The initial substrate is defined as

$$\Phi_s = \left[1 - \frac{2}{\pi} \arctan(y'/x') \right]/2,$$

where

$$x' = x \cos(\theta) + y \sin(\theta) - r \cos(\theta_0),$$

$$y' = -x \sin(\theta) + y \cos(\theta),$$

and

$$r = \sqrt{x^2 + y^2}$$

with $\theta = 200°$ and $\theta_0 = 60°$. Figure 1(a) shows the substrate image. Two steps emerge from the center of the x-y domain
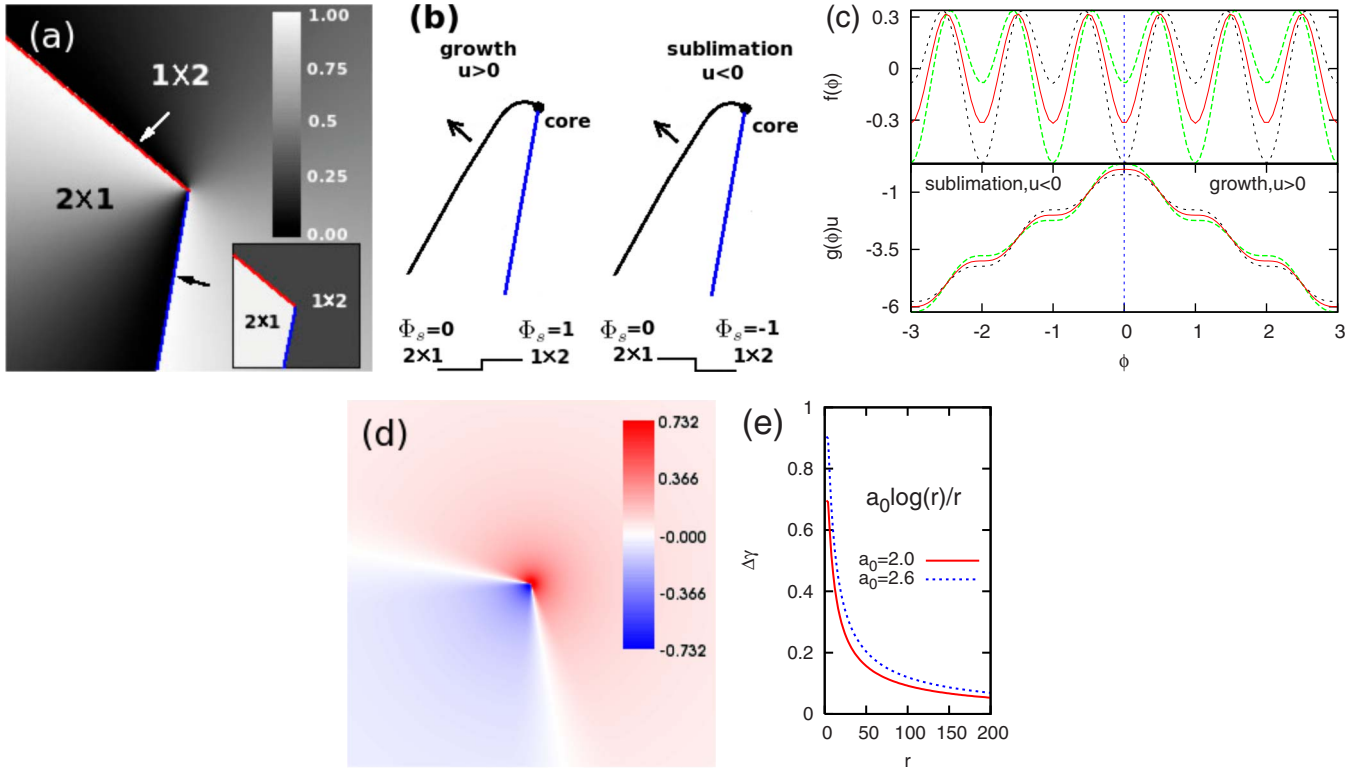
FIG. 1. (Color online) (a) The image of the initial substrate on a square domain of area $(450 \times 450)a^2$. The gray denotes the surface height, and the sharp change in gray indicates the position of the step. Two steps emerge from the center along the red line (denoted by the white arrow) and the blue line (denoted by the black arrow). Two terraces are exposed, terminated by the (2×1) phase (denoted by bright in the inset) and the (1×2) phase (denoted by dark in the inset), respectively. The change in contrast from bright to dark in the inset also indicates the position of the step. (b) The step structure described by the phase-field variable. (c) The phenomenological free-energy density functions. (d) The distribution of $\Delta\gamma$ that describes difference in the surface energy of the (2×1) and (1×2) phases. (e) The magnitude of $\Delta\gamma$, being taken as $a_0 \log(r)/r$ according to the distance to the center of the domain. Here, $f(\phi)$, $g(\phi)u$, $\Delta\gamma$, and r are dimensionless quantities after normalization.

(i.e., the core of the screw dislocation). The blue step (denoted by the black arrow) locates in the lower part of the x-y domain, and the red step (denoted by the white arrow) locates in the upper part of the x-y domain. Two terraces are exposed, being terminated by the (2×1) and (1×2) phases, respectively. In Fig. 1(b), we explain the Φ field around the blue step (denoted by the black arrow) for the surface growth and sublimation. The step direction in the case of surface growth is chosen opposite to that of surface sublimation. We choose $\Phi_s = 0$ as the downside terrace and $\Phi_s = 1$ as the upside terrace in the case of surface growth while we choose $\Phi_s = 0$ as the upside terrace and $\Phi_s = -1$ as the downside terrace in the case of surface sublimation. Thus, for the two cases of surface growth and sublimation, the directions of step motion are identical (clockwise, denoted by the arrows), and the corresponding phase switching are the same, being $(2 \times 1) \rightarrow (1 \times 2)$.

Besides, we define the dimensionless adatom density as $u = (c - c_{eq})\Omega$, wherein c is the adatom density (in units of atom/cm^2), c_{eq} is the equilibrium adatom density at a straight step, the atomic area $\Omega = a^2$, and a is the atomic lattice constant. As a starting point, the dimensionless free-energy functional is formulated as

$$H = \int dV \left[\frac{1}{2} W'^2 (\nabla_{r'} \Phi)^2 + f(\phi)/\pi + \lambda g(\phi)u/\pi \right], \quad (1)$$

where $\phi = \Phi - \Phi_s$. Initially, $\phi = 0$ indicates the substrate. In the case of surface growth ϕ tends to increase for the positive driving force of the adatom density, i.e., $u > 0$, and $\phi = 1, 2, 3, \ldots$ describe the grown overlayers whose atomic-layer heights starting from the substrate are one, two, three (atomic layers), and so on. In the case of surface sublimation ϕ tends to decrease for $u < 0$, and $\phi = -1, -2, -3, \ldots$ describe the thickness of the atomic layers that are removed from the substrate. The surface is terminated alternatively by (1×2) and (2×1) for neighboring atomic-layer heights. In the x-y region where the terrace is initially terminated by (2×1), as denoted by the bright field in the inset of Fig. 1(a), $\phi = 0$ corresponds to (2×1), and then $\phi = \pm 1, \pm 3, \pm 5, \ldots, \pm 2n+1$ corresponds to (1×2) while $\phi = \pm 2, \pm 4, \ldots, \pm 2n$ corresponds to (2×1). In the x-y region where the terrace is initially terminated by (1×2), as denoted by the dark field in the inset of Fig. 1(a), $\phi = 0$ corresponds to (1×2), and then $\phi = \pm 1, \pm 3, \pm 5, \ldots, \pm 2n +1$ corresponds to (2×1) while $\phi = \pm 2, \pm 4, \ldots, \pm 2n$ corresponds to (1×2).

The functions $f(\phi)$ and $g(\phi)$ are written as

$$f(\phi) = -\cos(2\pi\phi) \pm \Delta\gamma\cos(\pi\phi), \qquad (2)$$

$$g(\phi) = \sin(2\pi\phi) - 2\pi\phi \pm \Delta\gamma\cos(\pi\phi), \qquad (3)$$

where we use the parameter $\Delta\gamma$ to describe the difference in the surface energy of (2×1) and (1×2), i.e., $\Delta\gamma = \gamma_{2\times1} - \gamma_{1\times2}$. The distribution of $\Delta\gamma$ corresponds to the strain field of the screw dislocation. The sign of the $\Delta\gamma$ term in $f(\phi)$ and $g(\phi)$ has two options. In the case of surface growth, "+" is chosen in the x-y region where the terrace is initially terminated by (2×1), and "−" is chosen in the x-y region where the terrace is initially terminated by (1×2). In the case of surface sublimation, the sign of $\Delta\gamma$ term in $g(\phi)$ is changed into "∓" in order to consider that the step direction chosen for the surface sublimation is opposite to that for the surface growth [as illustrated in Fig. 1(b)]. Here, − refers to the x-y region where the terrace is initially terminated by (2×1), and + refers to the x-y region where the terrace is initially terminated by (1×2).

Figure 1(c) demonstrates $f(\phi)/\pi$ and $g(\phi)u/\pi$ with $u = 1, -1$, and $\Delta\gamma = 0, 0.732, -0.732$. The red (dark gray) solid lines correspond to $\Delta\gamma = 0$. The green (light gray) dashed lines correspond to $+\Delta\gamma$ with $\Delta\gamma > 0$ or $-\Delta\gamma$ with $\Delta\gamma < 0$ while the black dotted lines correspond to $-\Delta\gamma$ with $\Delta\gamma > 0$ or $+\Delta\gamma$ with $\Delta\gamma < 0$. The green (light gray) dashed lines indicate that $\phi = \pm1, \pm3, \pm5, \ldots, \pm2n+1$ are the energy-preferred growth points, i.e., $f(\phi)/\pi$ is of lower minimums and $g(\phi)u/\pi$ is of steeper potential variations at $\phi = \pm1, \pm3, \pm5, \ldots, \pm2n+1$ than those at $\phi = 0, \pm2, \pm4, \ldots, \pm2n$. In contrast, the black dotted lines illustrate that $\phi = 0, \pm2, \pm4, \ldots, \pm2n$ are the energy-preferred growth points. According to the specific surface-termination meanings of ϕ in the different regions of the simulation domain, $f(\phi)$ and $g(\phi)$ describe the energetically favored growth of (1×2) when $\Delta\gamma > 0$ as well as the energetically favored growth of (2×1) when $\Delta\gamma < 0$ on the whole domain. In Fig. 1(c), the right half corresponds to the surface growth for $u > 0$, and the left half corresponds to the surface sublimation for $u < 0$. Figure 1(c) is bilateral symmetrical, indicating that $f(\phi)$ and $g(\phi)$, as formulated by Eqs. (2) and (3), can describe both cases of surface growth and sublimation.

The basic equations for surface growth are then written as

$$\tau'\frac{\partial\Phi}{\partial t'} = -\frac{\delta H}{\delta\Phi} = W'^2\nabla_{r'}^2\Phi - [2\sin 2\pi\phi \pm \Delta\gamma\sin(\pi\phi)$$
$$- \lambda u(2\cos 2\pi\phi) - 2 \mp \Delta\gamma\sin(\pi\phi)], \qquad (4)$$

$$\frac{\partial u}{\partial t'} = D\nabla_{r'}^2 u - \frac{\partial\Phi}{\partial t'} + F, \qquad (5)$$

where r' represents the spatial coordinates, and t' is the time; W' represents the width of the phase-field transition zone, τ' is the characteristic time of attachment of adatoms at steps, and λ is a dimensionless coupling constant; D is the diffusion rate of the dimension Ω/s, and F is the deposition rate of adatoms of the dimension monolayer (ML)/s (i.e., $1/\Omega$ s).

By using the expressions defined by

$$\vec{r} = (x,y) = \frac{\vec{r}'}{\Omega}, \quad t = \frac{t'}{\Omega/D},$$

$$W = \frac{W'}{a}, \quad \tau = \frac{\tau'}{\Omega/D}, \qquad (6)$$

the dimensionless governing equations are further rewritten as

$$\tau\frac{\partial\Phi}{\partial t} = W^2\nabla_r^2\Phi - [2\sin 2\pi\phi \pm \Delta\gamma\sin(\pi\phi)$$
$$- \lambda u(2\cos 2\pi\phi) - 2 \mp \Delta\gamma\sin(\pi\phi)], \qquad (7)$$

$$\frac{\partial u}{\partial t} = \nabla_r^2 u - \frac{\partial\Phi}{\partial t} + \frac{F}{D}. \qquad (8)$$

To better describe the actual deposition of adatoms, we restore its randomness on the surface and discreteness in time by modifying the F/D term, and hence re-express Eq. (8) as

$$\frac{\partial u}{\partial t} = \nabla_r^2 u - \frac{\partial\Phi}{\partial t} + \delta(\vec{r} - \vec{r}_i)\delta(t - t_i), \qquad (9)$$

where $\vec{r}_i$ is chosen randomly on the simulation domain of the dimensionless size S, and t_i is discretized by the time interval, $\Delta t_d = D/(FS)$. The effect arising from the third term on the right-hand side of Eq. (9) is equivalent to F/D in the simulations of large deposited coverages. With the sign of the last term in Eq. (7) being $\pm$ and the sign of the last term in Eq. (9) being −, the governing equations are changed to describe surface sublimation.

By following the *thin-interface asymptotic analysis*,[14] we determine the phase-field model parameters according to

$$\lambda = a_1\frac{W}{d_0}, \quad \tau = a_1 a_2\frac{W^3}{d_0}, \qquad (10)$$

where $a_1 = 0.36$, $a_2 = 0.51$, and the dimensionless capillary length is defined as $d_0 = \Omega ac_{eq}\sigma/k_B T$. Here, σ is the step stiffness, k_B is the Boltzmann constant, and T is temperature. In the phase-field simulation, a value of W is first inputted in the limit that W is thin, and then the other model parameters are determined according to Eq. (10).[10]

In our simulations, $W = 3$, $\lambda = 8\times10^3$, and $\tau = 3\times10^4$ are chosen referring to $d_0 = 10^{-4}$ for the qualitative simulation of the Si(001) system. The growth conditions are chosen as $D = 10^4$ Ω/s and $F = 0.0002 - 0.04$ ML/s, whose ratio, F/D, is inputted into the dimensionless time interval, Δt_d, in Eq. (9). Usually epitaxy occurs at room temperature or above, where diffusion of adatoms is active, i.e., D is far larger than zero. Generally speaking, F/D can be taken as finite value. Here, F/D is chosen around $2\times10^{-8} - 4\times10^{-6}$, indicating the non-equilibrium growth conditions. Referring to the distribution of $\Delta\gamma$ used in the literature,[4] we choose $\Delta\gamma$ as shown in Fig. 1(d), where $\Delta\gamma$ is negative, taken as $-a_0\log(r)/r$, in the third quadrant (left lower quadrant) and turns positive, i.e., $a_0\log(r)/r$ in the first, second, and fourth quadrants (the other quadrants) across the thin smoothing areas, where r is the distance to the center of the simulation domain. We ad-

just the value of $\Delta\gamma$ in terms of the coefficient a_0 phenomenologically. With a_0 being 2.2 and 2.6, Fig. 1(e) illustrates the values of $\Delta\gamma$ used in our simulation. The anisotropy of Si(001) surfaces is neglected in our model with the effect of $\Delta\gamma$ being considered.

Equations (7) and (9) are solved on the domain of S $=450\times450$ using a second-order finite difference method on uniform Cartesian grids with a first-order finite difference approximation for the time. The spatial grid spacing Δx $=1.5$ and time step Δt is chosen as $\Delta t < \min[(\Delta x)^2/5, \Delta t_d]$, and is small enough to ensure that variation in Φ is less than one in one time step. We use Neumann boundary condition in all directions. The simulated Φ field demonstrates the step profile, where the sharp transition zone of Φ indicates the position of the step. Besides, the Φ field also represents the image of the surface termination according to the specific surface-termination meaning of Φ or ϕ on the simulation domain. In the experiment,[4] the step profile on the Si(001) surfaces is obtained using low-energy electron microscopy (LEEM), where the (2×1) phase appears bright, whereas the (1×2) phase appears dark, and thus the position of the step is indicated by the change in contrast from bright to dark. Referring to the LEEM imaging, we also check the step profile in terms of the surface-termination phase.

All simulations are conducted for large coverages so that the spiral growth approaches the steady state. The deposited coverage, θ, is around 5–200 ML for F $=0.0002–0.04$ ML/s. When the characteristic step spacing almost keeps constant with increasing coverage of adatoms, or when the characteristic step spacing from the center is only a few percent smaller than the asymptotic step spacing far from the core, we can judge that the spiral growth has already reached the steady state. The step spacing is measured directly on the visual image of the simulated step morphology. Besides, the height-height correlation function of the simulated step morphology is calculated, where the correlation length also indicates the step spacing.

III. RESULTS AND DISCUSSION

Our simulations reproduce the anomalous step motion on the Si(001) surface. First, as shown in Figs. 2(a)–2(c), the step growth is suppressed near the core because both the $(1\times2)\rightarrow(2\times1)$ switching at the red step (denoted by the white arrow in the inset) and the $(2\times1)\rightarrow(1\times2)$ switching at the blue step (denoted by the black arrow in the inset) are unfavored, which causes the S-shaped profile having positive curvature near the core, as denoted by the arrows in Fig. 2(c). Next, as shown in Figs. 2(d)–2(f) the step growth turns to speed up when the two steps enter into their energy-favored areas. The blue step (denoted by the black arrow in the inset) grows fast in the first, second, and fourth quadrants where $\Delta\gamma > 0$, and the red step (denoted by the white arrow in the inset) grows fast in the third quadrant where $\Delta\gamma < 0$. In Fig. 2(f), one cycle is completed, and the step profile exactly repeats the pattern in Fig. 2(a). The simulation for the surface sublimation represents the same profile but with the opposite step direction.

The spiral step growth is simulated for different distributions of $\Delta\gamma$. The case of zero $\Delta\gamma$ corresponds to Si(111),
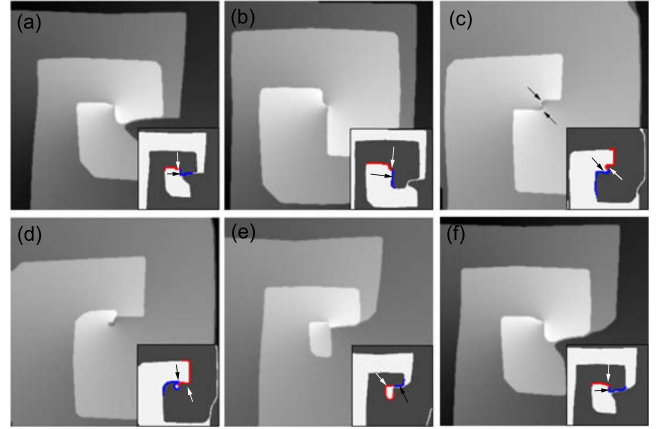

FIG. 2. (Color online) Images of the spiral growth simulated for $\theta=3.3$, 3.7, 4.3, 4.5, 4.9, and 5.3 MLs in (a)–(f) using nonzero $\Delta\gamma$, where $a_0=2.0$, $F=0.0002$ ML/s, and the domain area is $(450\times450)a^2$. The lightest gray corresponds to the highest surface height, being around 5 atomic layers (ALs) in (a)–(c), 6 ALs in (d), and 7 ALs in (e) and (f). The sharp change in gray indicates the position of the step. The corresponding simulated images of the surface terminations are shown in the insets, where the (2×1) and (1×2) phases are denoted by bright and dark, respectively, and the position of the step is indicated by switching between bright and dark.

nonreconstructed semiconductors, and metal surfaces. Here, the step represents the conventional Archimedes spiral shape with regular arrangement of (1×2) and (2×1), as shown in Fig. 3(a). In the case of nonzero $\Delta\gamma$, as shown in Figs. 3(b) and 3(c), the spiral growth is anomalous, representing the wavy step ridges with a positive curvature near the center. In spite of the irregular spiral profile, the width of one couple of (1×2) and (2×1) almost keeps constant with the increasing polar angle. Therefore, we can define the average width of one couple of (1×2) and (2×1) as the step spacing l. In Fig. 3(b), l is about $120\Delta x$ (i.e., $180a$, where Δx corresponds to $1.5a$), being far larger than that, about $60\Delta x$ (i.e., $90a$), in Fig. 3(a). In Fig. 3(c), the positive curvature near the center becomes deeper, and larger l, about $190\Delta x$ (i.e., $285a$), is
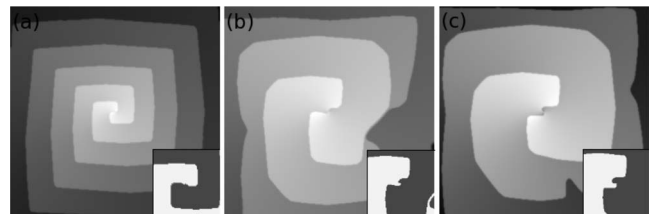

FIG. 3. Images of the spiral growth at the steady-state regime simulated using zero $\Delta\gamma$ in (a) and nonzero $\Delta\gamma$, $a_0=2.0$ in (b) and $a_0=2.6$ in (c), where $F=0.001$ ML/s, $\theta=22$ ML s, and the domain area is $(450\times450)a^2$. The lightest gray corresponds to the highest surface height, being around 24 ALs. The sharp change in gray indicates the position of the step. Inset: the corresponding simulated images (segment) of the surface termination, where the (2×1) and (1×2) phases are denoted by bright and dark, respectively, and the position of the step is indicated by switching between bright and dark.
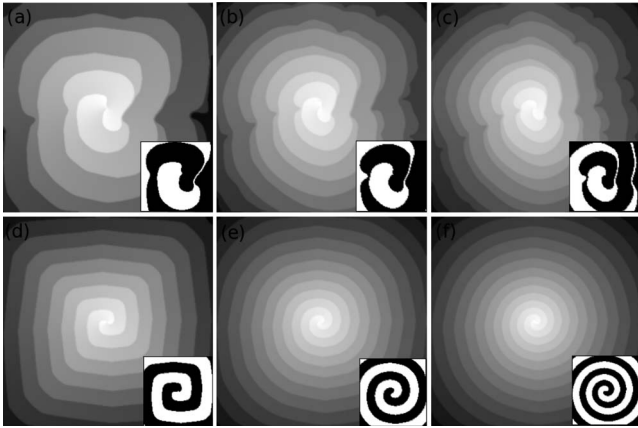
FIG. 4. Images of the spiral growth at the steady-state regime simulated using $F=0.005$ ML/s (left), 0.02ML/s (middle), and 0.04 ML/s (right) for nonzero $\Delta\gamma$ with $a_0=2.0$ in (a)–(c) and zero $\Delta\gamma$ in (d)–(f), where $\theta=105$ ML (left), 187 ML (middle), and 224 ML (right), and the domain area is $(450\times450)a^2$. The lightest gray corresponds to the highest surface height, being around 109, 193, 231, 111, 200, and 233 ALs in (a)–(f). The sharp change in gray indicates the position of the step. Inset (enlarged): the corresponding simulated images of the surface termination, where the (2×1) and (1×2) phases are denoted by bright and dark, respectively, and the position of the step is indicated by switching between bright and dark.

obtained for the larger $\Delta\gamma$ magnitude with $a_0=2.6$. This indicates that the nonzero $\Delta\gamma$ tends to reverse the curvature of the spiral ridge near the core and enlarge the step space. This effect is equivalent to a force that is opposite to the driving force of the step growth.

In Fig. 4, the spiral growth is further investigated for $F=0.005$, 0.02, and 0.04 ML/s. For all cases of F, the anomalous spiral profiles represent larger l than the general Archimedes ones. For the general Archimedes spiral growth, the step curvature remains negative along the whole step ridge. For the anomalous spiral growth, the step curvature near the core changes with F, being positive for $F=0.005$ ML/s but being negative for $F=0.02$ and 0.04 ML/s. This positive curvature indicates that the force arising from $\Delta\gamma$ prevails against the driving force of the step growth for the cases of small F, such as 0.005 ML/s, while the negative curvature indicates that the force arising from $\Delta\gamma$ is not prominent for the cases of large F, such as 0.02 and 0.04 ML/s.

The scaling law of $l\sim F^{-\alpha}$ is presented in Fig. 5. The scaling exponent α describes the step dynamics. For example, when desorption is fast and only adatoms deposited near a step are incorporated, $\alpha=1$ was predicted, indicating the local step dynamics.[1] Given the negligible desorption, $\alpha=1/3$ was predicted, indicating the nonlocal step dynamics in the diffusion field of adatoms on the whole surface, and $\alpha=1/2$ was predicted for the limited atomic attachment kinetics at the step.[2] As illustrated in Fig. 5, $\alpha=0.32$ is obtained in the simulations of zero $\Delta\gamma$, which is in agreement with the global diffusive dynamics, $\alpha=1/3$, of the general Archimedes spiral step growth. The scaling exponent, $\alpha=0.41$, is obtained for the anomalous spiral growth simulated
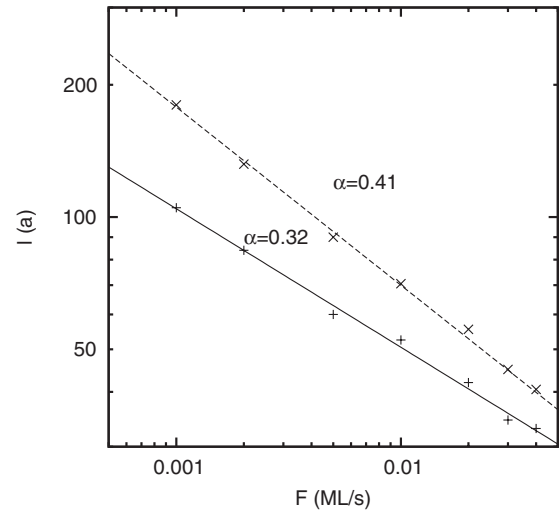

FIG. 5. The step spacing l as a function of F obtained for zero $\Delta\gamma(+)$ and nonzero $\Delta\gamma$ with $a_0=2.0$ ($\times$). The lines are the best fits for the power-law exponents $\alpha=0.32$ (solid) with the fitting error of 0.009 and $\alpha=0.41$ (dash) with the fitting error of 0.007.

in the case of nonzero $\Delta\gamma$ values of $a_0=2.0$. The force arising from nonzero $\Delta\gamma$ enlarges l greatly for the cases of small F but has weak effects on l for the cases of large F. This is consistent with the variation in the curvature near the core, being positive for $F=0.000-0.005$ ML/s but being negative for $F=0.02-0.04$ ML/s.

In the simulation of nonzero $\Delta\gamma$, the spiral step profile is dependent on the magnitude of $\Delta\gamma$ near the core but recovers the diffusion-dominant growth far from the core. A certain locality enters into the anomalous spiral step growth, which results in the deviation of α from the global diffusive dynamics. Since this locality is weak, it seems difficult to achieve a strong local step dynamics, such as $\alpha=1/2$, in our simulations. On the other hand, it seems unlikely to rule out the deviation of α because the effect of nonzero $\Delta\gamma$ that enlarges l is deepening with the decreasing F for the anomalous step motion. Therefore, Fig. 5 indicates a crossover tendency to local dynamics of anomalous spiral step growth on the Si(001) surface. Further works are needed in the future to check quantitatively if the crossover tendency changes with the magnitude and distribution of the strain field of the screw dislocation on the Si(001) surface.

Spiral step growth on Si(001) surfaces is checked further for other stress cases. As compared with Fig. 3(b), the spiral growth is simulated in Fig. 6(a) for a $\Delta\gamma$ distribution opposite to that shown in Fig. 6(d), i.e., $\Delta\gamma<0$ in the first, second, and fourth quadrants, and $\Delta\gamma>0$ in the third quadrant, which is another possible stress distribution caused by the different slip direction of the screw dislocation on the Si(001) surface.[4,15] The spiral step growth represents the same profile as that shown in Fig. 3(b) but with the upside-down arrangement of (1×2) and (2×1). The different slip direction of the screw dislocation may cause the different initial configuration. Our simulations show that, being independent of the initial step configuration, there is always one type of anomalous spiral profile, as shown in Fig. 6(a), but the arrangement of (1×2) and (2×1) is dependent on the
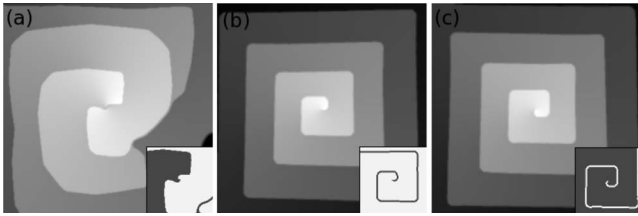
FIG. 6. Images of the spiral growth at the steady-state regime simulated for the possible $\Delta\gamma$ distributions, such as (a) $\Delta\gamma<0$ in the first, second, and fourth quadrants, and $\Delta\gamma>0$ in the third quadrant, (b) uniform distribution of $\Delta\gamma<0$, and (c) uniform distribution of $\Delta\gamma>0$, where $F=0.001$ ML/s, $\theta=22$ ML s, and the domain area is $(450\times450)a^2$. The lightest gray corresponds to the highest surface height, being around 24, 27, and 27 ALs in (a)–(c). The sharp change in gray indicates the position of the step. Inset: the corresponding simulated images of the surface termination, where the (2×1) and (1×2) phases are denoted by bright and dark, respectively, and the position of the step is indicated by switching between bright and dark.

slip direction. In Figs. 6(b) and 6(c) spiral step growth is simulated for a uniform distribution of $\Delta\gamma$. The uniform misfit stress is dominant in heteroepitaxy, such as Ge/Si epitaxy. In these cases, one of (1×2) and (2×1) is always favored. Our simulations represent the persisting step bunching, which forms double-atomic-layer steps and (2×1)-terminated terraces [in Fig. 6(b)] or (1×2)-terminated terraces [in Fig. 6(c)]. Here, the spiral step growth retrieves to the general Archimedes spiral profile.

The step motion that deviates from the general Archimedes spiral is also observed on other surfaces such as KH$_2$PO$_4$(KDP), *p*-nitrophenyl nitroxyl nitroxide, BaNO$_3$, SiC, GaN, and so on,[16–20] where the strain energy field near the screw dislocation leads to the positive step curvature near the dislocation outcrop as well as the hollow dislocation core.[21] We can find similarity between the anomalous spiral growth on the Si(001) surface and the growth of the hollow dislocation core. For example, the anomalous spiral motion

on the Si(001) surface causes the vacancy terrace at the dislocation core, as shown in Fig. 2(d), which resembles the experimental image of the hollow dislocation core that was shown in Fig. 1b of Ref. 14. In our simulations the vacancy terrace disappears soon, as accompanied by aggregation of the surrounding atomic overlayer. If the adatom density is low at the core, which may be caused by limited diffusion of adatoms to the core or strong desorption of adatoms, the vacancy terrace may survive or aggregate further to form the macrosteps of the hollow dislocation core.

IV. CONCLUSION

In summary, we extend a phase-field model of spiral step growth by considering surface phase switching between (1×2) and (2×1) on the Si(001) surface, and investigate spiral step motion on the Si(001) surface for possible strain distributions and a large range of deposition rates. Our simulations reproduce experimentally observed anomalous spiral step motion on a Si(001) surface. A scaling law $l\sim F^{-0.41}$ is obtained for the anomalous spiral step growth. This scaling law deviates from the earlier result for conventional spiral step growth, indicating the crossover toward the local step dynamics due to the strain field of the screw dislocation on the Si(001) surfaces. The phase-field model is advantageous and favorable in including other complex factors such as anisotropy, limited atomic attachment kinetics, and Ehrlich-Schwoebel barriers, which may further affect the spiral step growth on the Si(001) surfaces.

[1] W. K. Burton, N. Cabrera, and F. C. Frank, Philos. Trans. R. Soc. London, Ser. A **243**, 299 (1951).

[2] A. Karma and M. Plapp, Phys. Rev. Lett. **81**, 4444 (1998).

[3] A. Redinger, O. Ricken, P. Kuhn, A. Rätz, A. Voigt, J. Krug, and T. Michely, Phys. Rev. Lett. **100**, 035506 (2008).

[4] J. B. Hannon, V. B. Shenoy, and K. W. Schwarz, Science **313**, 1266 (2006).

[5] P. W. Voorhees, Science **313**, 1247 (2006).

[6] O. L. Alerhand, D. Vanderbilt, R. D. Meade, and J. D. Joannopoulos, Phys. Rev. Lett. **61**, 1973 (1988).

[7] F. K. Men, W. E. Packard, and M. B. Webb, Phys. Rev. Lett. **61**, 2469 (1988).

[8] F. Liu and H. Metiu, Phys. Rev. E **49**, 2601 (1994).

[9] Y. C. Xu and B. G. Liu, Phys. Rev. Lett. **100**, 056103 (2008); J. Phys. D: Appl. Phys. **42**, 035402 (2009).

[10] Y. M. Yu and B. G. Liu, Phys. Rev. E **69**, 021601 (2004).

[11] F. Otto, P. Penzler, A. Rätz, T. Ribalta, and A. Voigt, Nonlinear-

ity **17**, 477 (2004).

[12] T. Laurila, M. Pradas, A. Hernandez-Machado, and T. Ala-Nissila, Phys. Rev. E **78**, 031603 (2008).

[13] Y. M. Yu and B. G. Liu, Phys. Rev. B **77**, 195327 (2008).

[14] A. Karma and W.-J. Rappel, Phys. Rev. E **57**, 4323 (1998).

[15] X. H. Liu and K. W. Schwarz, Modell. Simul. Mater. Sci. Eng. **13**, 1233 (2005).

[16] J. J. De Yoreo, T. A. Land, and J. D. Lee, Phys. Rev. Lett. **78**, 4462 (1997).

[17] J. Fraxedas, J. Caro, A. Figueras, P. Gorostiza, and F. Sanz, Surf. Sci. **415**, 241 (1998).

[18] K. Maiwa, M. Plomp, W. J. P. Van Enckevort, and P. Bennema, J. Cryst. Growth **186**, 214 (1998).

[19] W. Qian, G. S. Rohrer, M. Skowronski, K. Doverspike, L. B. Rowland, and D. K. Gaskill, Appl. Phys. Lett. **67**, 2284 (1995).

[20] W. M. Vetter and M. Dudley, J. Appl. Phys. **96**, 348 (2004).

[21] F. C. Frank, Acta Crystallogr. **4**, 497 (1951).